Adaptive Interval Type-2 Fuzzy Fixed-time Control for Underwater Walking Robot with Error Constraints and Actuator Faults Using Prescribed Performance Terminal Sliding-mode Surfaces

Hongde Qin[1] · **He Yang**[1] · **Yanchao Sun**[1] · **Yuang Zhang**[1]

Abstract Underwater walking robot (UWR) is a kind of autonomous underwater vehicles which can walk underwater. In this work, the fixed-time tracking control problem of UWR with external disturbances, error constraints, and actuator faults is investigated. An interval type-2 fuzzy neural network approximator is designed to tackle nonlinear uncertainties, and a novel prescribed performance terminal sliding-mode surface is proposed to handle error constraints. Furthermore, two fault-tolerant controllers are given, where one is nonsingular and the other has higher steady-state precision. According to Lyapunov theory, the proposed controllers can guarantee that system states will converge to the expected values in a fixed time. Simulation results demonstrate the effectiveness of the proposed control strategies.

Keywords Underwater walking robot · Interval type-2 fuzzy logic system · Error constraint · Fixed-time control · Fault-tolerant control

1 Introduction

Over the past decades, autonomous underwater vehicles (AUVs) have been successfully applied in many fields, such as offshore oil and gas development [1], marine scientific research [2], and underwater structure inspection [3]. Most of the existing AUVs are screw-propelled. However, screw-propelled AUVs can hardly keep themselves safe near the coast, seabed, and underwater structures, where the terrains are rough [4]. Underwater walking robot (UWR) is a kind of bionic AUVs which is inspired by multi-legged animals [5]. By letting its each leg track a desired trajectory, UWR can walk on rough terrains underwater, which makes it have a broad prospect in many ocean applications.

Tracking errors of UWR's each leg should be constrained such that the legs will not collide with each other in the unknown underwater environment. Therefore, solving the control problems with error constraints of AUV, especially UWR has both theoretical and engineering values. Barrier Lyapunov function (BLF) is a common technique to deal with error constraints. There are many relevant researches [6–9] based on log-type and tan-type BLFs, and some other types are proposed in [10–12]. A log-type BLF was used to handle the tracking problem of AUV with constant error constraints in [13]. Fuzzy logic system (FLS) is a common technique to model nonlinear functions for underwater robot control [14]. The expert judgement can be integrated into FLS [15]. Compared with the neural network technique [16] [17], FLS has a smaller amount of computation due to making full use of engineer experience. In [18], a type-1 FLS was proposed to estimate and compensate the nonlinear uncertainties of AUV, and a controller based on the tan-type BLF was developed to ensure output constraints not violated. However, compared with type-2 FLS, type-1 FLS tackles the uncertainties less efficiently due to crisp antecedents and consequents of the rule base [19, 20]. Type-2 FLS has demonstrated outstanding performance in dealing with uncertainties [21]. Compared with type-1 FLS, type-2 FLS has better fuzzy dynamic adaptation in different applications [22]. Therefore, type-2 FLS can estimate and compensate the nonlinear uncertainties of UWR's leg more efficiently. Type-2

✉ Yanchao Sun
sunyanchao@hrbeu.edu.cn

1 Science and Technology on Underwater Vehicle Laboratory, Harbin Engineering University, Harbin 150001, China

FLS has superior performance in modeling and control [23]. In [24], the footprint of uncertainty in interval type-2 fuzzy sets was studied by nonlinear control theory, and it was theoretically explained that the controllers based on interval type-2 FLS can achieve better control performance. In [25], type-2 FLS was used to deduce center of mass correction to compensate for the error caused by model uncertainties and external disturbances, and an optimized control algorithm was proposed for bipedal robots. In [26], an interval type-2 fuzzy neural network (IT2FNN) approximator was proposed to approximate unknown nonlinear functions, and an adaptive backstepping controller was designed for a flexible-joint manipulator. Due to the high performance of interval type-2 FLS to deal with uncertain and nonlinear dynamics, an interval type-2 fuzzy logic controller was designed for the control of human-like robots' hydraulic actuator in [27]. In [28], general forms of interval type-2 FLSs were discussed and a type-2 FLS whose secondary grades can be nonconvex type-1 fuzzy sets was proposed. There are many works on type-2 fuzzy control for robots [29–33]. Prescribed performance (PP) is another method which is different from BLF. For handling error constraints, PP control scheme transforms the constrained system into an equivalent unconstrained system by introducing a performance function [34, 35]. Ref. [36] proposed a tracking control algorithm based on PP method for AUV with error constraints. A robust controller based on PP method and neural network technique was proposed in [37], and it guaranteed the tracking errors of AUV satisfied the prescribed constraints. In [38], PP control scheme was used to deal with error constraints. Although the error constraint problem is discussed, BLF and PP both have complex processes of controller design and stability analysis. For UWR's leg control, we expect to develop a simpler control strategy.

In addition to error constraints, there are still several challenges in practice. First, the control schemes for AUV in [39–41] were asymptotic, which implied that system states would not converge to the expected values until settling time was infinite. Due to the infinite settling time, the controller which only guarantees asymptotic convergence will adversely affect the control performance of UWR's leg. To achieve finite-time convergence, finite-time approaches have been developed in recent years [42]. Ref. [43] proposed a robust finite-time attitude controller based on the sliding-mode control (SMC) method. In [44], FLS was used to compensate uncertainties, and a finite-time control strategy based on nonsingular terminal sliding-mode control (TSMC) method was proposed for AUV. However, with the finite-time approach, the upper bound of settling time is influenced by the initial values of system states and cannot be determined in advance. Fixed-time control strategies which guarantee the upper bound of settling time to be independent of the initial conditions were proposed in [45] and [46]. Ref. [47] developed a fixed-time control scheme based on TSMC for nonlinear systems. However, there are few researches about fixed-time approaches for ocean robots [48]. Actuator fault is another main challenge for the control of UWR's leg in practice. In [49], a backstepping controller was designed for an underwater robot to track a desired spatial trajectory, and an additional fault detection unit was proposed to deal with actuator faults. Ref. [50] proposed a fault diagnosis method based on the Gaussian particle filter to address the actuator faults of AUV. However, it needed priori threshold values to identify the faults. However, both the fault detection and the fault diagnosis will increase the risk of system instability since the fault compensation time is delayed. In [51], type-2 FLS was used to approximate the nonlinear uncertainties caused by actuator faults, and an adaptive backstepping controller was proposed. In [52–54], adaptive technique and SMC method were used to handle the fault-tolerant control problem of AUV, and no additional observer was required to provide the feedback of fault information. However, how to design a novel fault-tolerant control scheme with fixed-time stability and error constraints for UWR's leg is still a difficulty.

This paper mainly investigates the fixed-time tracking control of UWR's leg with error constraints and actuator faults. Meanwhile, environment disturbance and unmodeled dynamics are also taken into account. First, an interval type-2 fuzzy neural network (IT2FNN) approximator is designed to tackle nonlinear uncertainties. In the controller design, we propose a nonsingular control strategy based on prescribed performance terminal sliding-mode control (PPTSMC) method. Furthermore, an integral PPTSMC strategy is proposed to reduce steady-state errors. The main contributions and originality of this study are stated as follows:

1. A novel prescribed performance terminal sliding-mode surface (PPTSMS) is designed to solve the error constraint problem. Due to the PPTSMS, state variables never violate the constraints of performance functions. What's more, the settling time of the state variables have a fixed bound once the surface has been reached.

2. Two PPTSMC strategies are proposed. They are robust and can guarantee fixed-time convergence, where one is nonsingular and the other has higher steady-state precision. Compared with the fixed-time approaches combined with BLF method and PP method, the fixed-time error constraint controller based on PPTSMC has an easier design process.

3. For each control strategy, the nonlinear uncertainties are approximated and compensated by an IT2FNN

approximator, and the adaptive law is developed to handle the approximation errors.

4. We consider the actuator faults in the tracking control of UWR's leg, and the additional observer which will increase the computational burden of the system is not required.

The rest of this research is organized as follows. Section 2 presents the background and preliminaries. Two controllers based on PPTSMC method are proposed in Sect. 3. In Sect. 4, we take simulation studies to demonstrate the effectiveness of the proposed methods. The conclusion of this research is given in Sects. 5.

2 Background and Preliminaries

### 2.1 Basic Mathematical Notations

Notations used in this study are defined in Table 1

2.2 Dynamical Model

Since the UWR needs to work on the rough underwater terrains, structural reliability and hydraulic property should be considered in the design process of UWR. Therefore, an UWR inspired by the crab is presented in Fig. 1. To walk underwater, each leg of UWR is required to track its own desired trajectory. One effective design of the UWR's legs is shown in Fig. 2. The dynamics of UWR's leg with

Table 1 Notations and definitions

Notation	Definition
$\|\mathbf{x}\|$	1-norm of the vector $x \in \mathcal{R}^n$
0_n	n-dimensional column vector with all elements being 0
sgn(·)	sign function, $\mathrm{sgn}(\cdot) = \begin{cases} 1, & \cdot > 0 \\ 0, & \cdot = 0 \\ -1, & \cdot < 0 \end{cases}$
$\mathrm{sig}^k(\cdot)$	$\mathrm{sig}^k(\cdot) = \| \cdot \|^k \mathrm{sgn}(\cdot)$ for $k > 0$
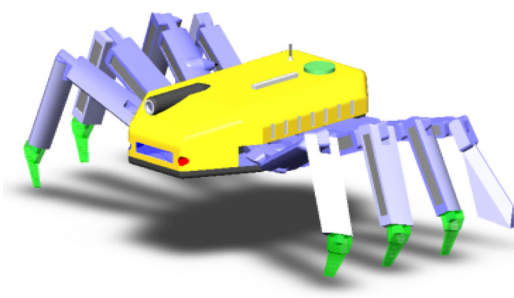
Fig. 1 UWR model
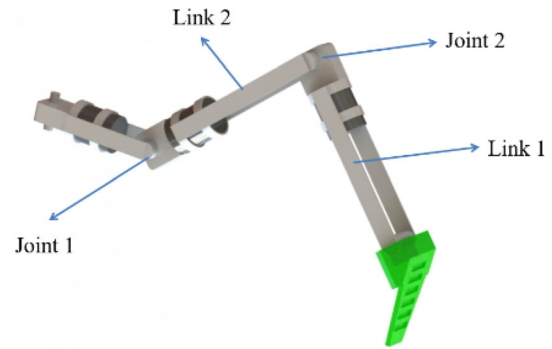
Fig. 2 UWR's leg model

p links can be described by Euler–Lagrange equation as follow

$$\mathbf{M}(\mathbf{q})\ddot{\mathbf{q}} + \mathbf{C}(\mathbf{q}, \dot{\mathbf{q}})\dot{\mathbf{q}} + \mathbf{g}(\mathbf{q}) = \boldsymbol{\tau} + \boldsymbol{\omega} \qquad (1)$$

where $\mathbf{q}, \dot{\mathbf{q}}, \ddot{\mathbf{q}} \in \mathcal{R}^p$ denote the generalized coordinate, velocity, and acceleration, respectively, $\mathbf{M}(\mathbf{q}) \in \mathcal{R}^{p \times p}$ represents the symmetric positive definite inertia matrix, $\mathbf{C}(\mathbf{q}, \dot{\mathbf{q}}) \in \mathcal{R}^{p \times p}$ represents the Coriolis and centrifugal matrix, $\mathbf{g}(\mathbf{q}) \in \mathcal{R}^p$ represents the gravitational force, $\boldsymbol{\tau} \in \mathcal{R}^p$ is the control input, and $\boldsymbol{\omega} \in \mathcal{R}^p$ is the external disturbance (including environment disturbance and unmodeled dynamics).

Property 1 *The inverse of the matrix* $\mathbf{M}(\mathbf{q})$ *is bounded, and there exists a positive constant* k_m *such that* $\|\mathbf{M}^{-1}(\mathbf{q})\| \le k_m$.

Assumption 1 The external disturbance $\boldsymbol{\omega}$ is bounded, and there exists a positive constant k_ω such that $\|\boldsymbol{\omega}\| \le k_\omega$.

Actuator fault is a common problem during the control process of the UWR's leg. The additional control input due to the actuator faults is defined as $\Delta\boldsymbol{\tau}$. Thus, the real control input acting on the UWR's leg is changed from $\boldsymbol{\tau}$ to $\boldsymbol{\tau} + \Delta\boldsymbol{\tau}$.

$$\boldsymbol{\tau} + \Delta\boldsymbol{\tau} = \boldsymbol{\rho}(t)\boldsymbol{\tau} + \boldsymbol{\tau}_b(t) \qquad (2)$$

where $\boldsymbol{\rho}(t) \in \mathcal{R}^{p \times p}$ is a diagonal matrix consisting of $\rho_i(t) \in [0, 1]$, $i = 1, 2, \ldots p$ as diagonal elements, which is used to describe the actuator effectiveness, and $\boldsymbol{\tau}_b(t) \in \mathcal{R}^p$ represents the actuator bias faults.

Assumption 2 The additional control input $\Delta\boldsymbol{\tau}$ is bounded, and there exists a positive constant k_δ such that $\|\Delta\boldsymbol{\tau}\| \le k_\delta$.

Rewriting the dynamics model (1), we have

$$\ddot{\mathbf{q}} = \mathbf{M}^{-1}(\mathbf{q})(\boldsymbol{\tau} - \mathbf{C}(\mathbf{q}, \dot{\mathbf{q}})\dot{\mathbf{q}} - \mathbf{g}(\mathbf{q})) + \mathbf{d} \qquad (3)$$

where $\mathbf{d} = \mathbf{M}^{-1}(\mathbf{q})(\Delta\boldsymbol{\tau} + \boldsymbol{\omega})$ represents nonlinear uncertainties. From Property 1, Assumptions 1, 2, we can obtain that $\mathbf{d}$ is bounded.

2.3 Definitions and Lemmas

Definition 1 [34] A smooth function $\rho(t) : \mathcal{R}_+ \to \mathcal{R}$ is called a performance function if

1. $\rho(t)$ is positive and decreasing,
2. $\lim_{t\to\infty} \rho(t) = \rho_\infty$, where ρ_∞ is a positive constant.

Lemma 1 [55] *Consider the system* $\dot{\mathbf{x}} = \mathbf{f}(\mathbf{x}(t))$, $\mathbf{x}(0) = \mathbf{x}_0 \in \mathcal{R}^n$, $\mathbf{f}(0_n) = 0$, *where* $\mathbf{f} : \mathbf{U}_0 \to \mathcal{R}^n$ *is a continuous function defined in an open neighborhood* $\mathbf{U}_0$ *of the origin. Suppose that there exists a Lyapunov function* $V(\mathbf{x}) : \mathbf{U}_0 \to \mathcal{R}_+$ *such that* $\dot{V}(\mathbf{x}) \le -\left(\alpha_0 V^{p_0}(\mathbf{x}) + \beta_0 V^{g_0}(\mathbf{x})\right)^{k_0} + \vartheta_0$, *where* $\dot{V}(\mathbf{x}) = \frac{\partial V(\mathbf{x})}{\partial t}$, $\alpha_0, \beta_0, p_0, g_0, k_0, \theta_0 \in \mathcal{R}_+$, $p_0 k_0 < 1$, *and* $g_0 k_0 > 1$. *Then the system is practically fixed-time stable. The setting time* T *satisfies* $T \le \frac{1}{\alpha_0^{k_0} \theta_0^{k_0}(1-p_0 k_0)} + \frac{1}{\beta_0^{k_0} \theta_0^{k_0}(g_0 k_0-1)}$, *and the convergence neighborhood can be presented as* $\left\{ \lim_{t\to T} \left| V(x) \le \min\left\{ \alpha_0^{-\frac{1}{p_0}} \left(\frac{\vartheta_0}{1-\theta_0^{k_0}}\right)^{\frac{1}{k_0 p_0}}, \right.\right.$ $\left.\left. \beta_0^{-\frac{1}{p_0}}\left(\frac{\vartheta_0}{1-\theta_0^{k_0}}\right)^{\frac{1}{k_0 g_0}}\right\}. \right\}$, *where* $0 < \theta_0 < 1$.

Remark 1 With proper parameters, Lemma 1 can guarantee the state variables to converge to an arbitrarily small neighborhood of the origin.

Lemma 2 [56] *For* $x_i \in \mathcal{R}$, $i = 1, 2, \ldots, n$, *we have*

$$\sum_{i=1}^n |x_i|^{\lambda_0} \ge \begin{cases} \left(\sum_{i=1}^n |x_i|\right)^{\lambda_0}, & 0 < \lambda_0 \le 1 \\ n^{1-\lambda_0}\left(\sum_{i=1}^n |x_i|\right)^{\lambda_0}, & \lambda_0 > 1 \end{cases}$$

2.4 Problem Formulation

Aiming at solving the tracking control problem of the UWR's leg, this research considers the dynamical model (3) with external disturbances, error constraints, and actuator faults, and designs control laws such that

1. *Tracking errors are guaranteed to converge in a fixed time.*
2. *Tracking errors never violate the constraints of performance functions.*
3. *The system remains stable whether the actuators fault or not.*

3 Control Law Design

To solve the control problem as previously mentioned, we propose two control algorithms and present our main contributions in this section. First, an IT2FNN approximator is proposed for the UWR's leg with uncertainties. Then a novel terminal sliding-mode surface is proposed, which is inspired by the BLF technique and the PP technique. Moreover, a novel nonsingular PPTSMC strategy with global fixed-time stability is proposed. Furthermore, a novel integral PPTSMC strategy is given to reduce steady-state errors. The details are as follows.

3.1 IT2FNN Approximator

In the study, an IT2FNN is used to deal with the nonlinear uncertainties $\mathbf{d}$ as a result of its good approximation capabilities. We propose the IT2FNN approximator as shown in Fig. 3, and we have

$$\mathbf{d} = \mathbf{W}^{\mathrm{T}}\varphi + \boldsymbol{\theta} \tag{4}$$

where $\mathbf{W}^{\mathrm{T}} = [\mathbf{w}_1, \mathbf{w}_2, \ldots, \mathbf{w}_n] = \left[\mathbf{w}'_1, \mathbf{w}'_2, \ldots, \mathbf{w}'_p\right]^{\mathrm{T}} \in \mathcal{R}^{p\times N}$ is the ideal weight matrix, $\boldsymbol{\theta} \in \mathcal{R}^p$ is the approximation error, and $\varphi = [\varphi_1, \varphi_2, \ldots, \varphi_n]^{\mathrm{T}} \in \mathcal{R}^N$ is the activation function vector with

$$\varphi_i = \frac{\underline{f}_i + \bar{f}_i}{\Sigma_{j=1}^n \left(\underline{f}_j + \bar{f}_j\right)}, \quad i = 1, 2, \ldots, N \tag{5}$$

where $\underline{f}_i$ and $\bar{f}_i$ denote the lower and upper bounds of the ith rule's firing strength for the input $x_1, x_2, \ldots, x_m$, respectively, and there are

$$\underline{f}_i = \prod_{k=1}^m \mu_{\underline{X}_k^i}(x_k) \tag{6}$$

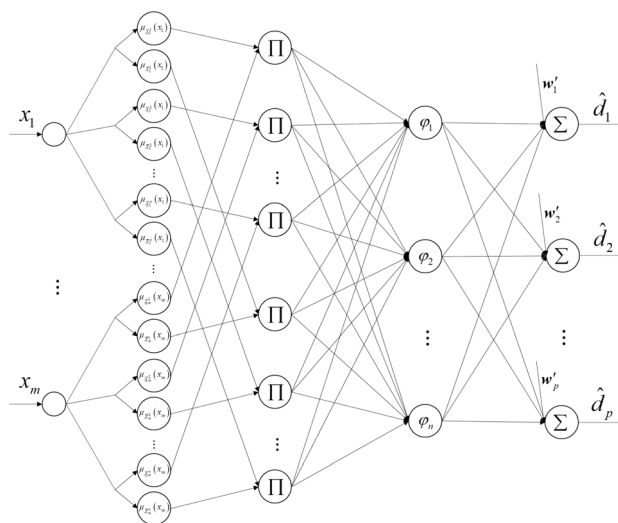$$\bar{f}_i = \prod_{k=1}^m \mu_{\bar{X}_k^i}(x_k) \tag{7}$$
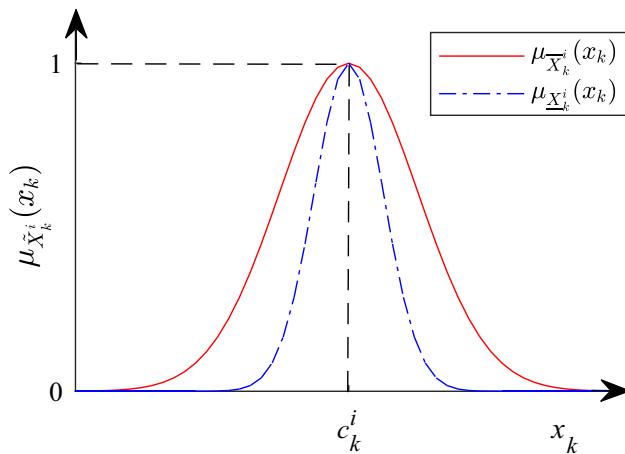

Fig. 3 IT2FNN system

Fig. 4 Gaussian membership function

where $\mu_{\underline{X}_k^i}(x_k)$ and $\mu_{\overline{X}_k^i}(x_k)$ denote the lower and upper membership functions (MF), respectively. Gaussian membership function is used in this study, as shown in Fig. 4.

Remark 2 The two most commonly used MFs for IT2FNN are Gaussian function and trapezoidal function. The Gaussian MF is always continuous. The trapezoidal MF is easier to analyze than the Gaussian MF but requires more parameters.

Assumption 3 Each link of the UWR's leg has similar dynamic characteristics. Thus the similar IF–THEN rules which have the same antecedents but different consequents can be used for each link.

The ith rule $(i = 1, 2, \ldots, N)$ in the IT2FNN approximator is defined as

R^i : if x_1 is $\tilde{X}_1^i$ and x_2 is $\tilde{X}_2^i$ and... and x_m is $\tilde{X}_m^i$, then $\mathbf{y}_i = \mathbf{w}_i$

$$(8)$$

where $[x_1, x_2, \ldots, x_m] = [q^T, \dot{q}^T]$, $\tilde{X}_k^i$, $k = 1, 2, \ldots, m$ denote the interval type-2 fuzzy sets, and $\mathbf{w}_i$ is the coefficient vector of output $\mathbf{y}_i$.

Remark 3 (8) is a simplification of Takagi–Sugeno-Kang rule, which combines with Assumption 3. The choices of rules' antecedents relay on practical experience and the values of rules' consequents $\mathbf{w}_i$ will be given by the adaptive technique later.

Assumption 4 The approximation error $\boldsymbol{\theta}$ is bounded, and there exists a positive constant Λ such that $\|\boldsymbol{\theta}\| \leq \Lambda$.

Remark 4 Type-2 FLS tackles the uncertainties more efficiently than type-1 FLS due to regarding fuzzy sets as fuzzy membership. Interval type-2 FLS and general type-2 FLS are two major kinds of type-2 FLS. Interval type-2 FLS has a simpler structure due to its fuzzy membership, which means it has the less computational burden.

3.2 Design of Nonsingular PPTSMC Strategy

We first define the following tracking error

$$\mathbf{e} = \mathbf{q} - \mathbf{q}_d \tag{9}$$

where $\mathbf{e} = [e_1, e_2, \ldots, e_p]^T$, and $\mathbf{q}_d \in \mathcal{R}^p$ denotes the desired trajectory.

To prevent constraint violation, we propose a novel PPTSMS for the ith link $(i = 1, 2, \ldots, p)$ of the UWR's leg as follows

$$s_i = -\frac{k_1 \sigma(e_i)}{\ln|e_i/a_i(t)|} + k_2 \dot{e}_i \tag{10}$$

where $k_1, k_2 > 0$, $a_i(t)$ is a performance function, and σ is a smooth function defined as

$$\sigma(x) = \frac{e^{\alpha x} - 1}{e^{\alpha x} + 1}, \ \alpha > 0 \tag{11}$$

Assumption 5 The initial values of tracking errors do not violate the constraints of performance functions, that is $|e_i(0)| < a_i(0)$.

Lemma 3 *Tracking errors never violate the constraints of performance functions due to the PPTSMS* (10). *Once state variables reach the surface* $s_i = 0$, *tracking errors are guaranteed to converge in a fixed time* T_{si}. *The settling time* T_{si} *is independent of the initial conditions and satisfies.*

$$T_{si} < \frac{k_2 a_i(0)}{k_1 \sigma(\xi_i)} \tag{12}$$

where $\xi_i \in (0, a_i(0))$ is a positive constant, which relies on α.

Proof Choose the Lyapunov function as follow

$$V_i = \frac{1}{2} s_i^2 \tag{13}$$

From (10, 13), and Assumption 5, the initial value of the Lyapunov function $V_i(0)$ is a positive constant. According to Lyapunov's stability theory, we have $V_i(t) \leq V_i(0)$. While $V_i \to +\infty$ when $e_i \to \pm a_i(t)$, which is contradictory. Thus, tracking errors never violate the constraints of performance functions, that is, $|e_i(t)| < a_i(t)$.

Differentiating (10), we can obtain that

$$\dot{s}_i = \psi_i + k_2 \ddot{e}_i \tag{14}$$

where $\psi_i = \frac{-k_1}{\ln|e_i/a_i(t)|(\exp(\alpha e_i)+1)} \left(\frac{2\alpha \exp(\alpha e_i)\dot{e}_i}{\exp(\alpha e_i)+1} - \frac{\dot{e}_i a_i(t) - e_i a_i'(t)}{\ln|e_i/a_i(t)|a_i(t)} \frac{\exp(\alpha e_i)-1}{|e_i|} \right)$. It can be found that (10) is nonsingular due to $\ln\left|\frac{e_i}{a_i(t)}\right| \neq 0$ and $\lim_{e_i \to 0} \frac{\exp(\alpha e_i)-1}{e_i} = \alpha$.

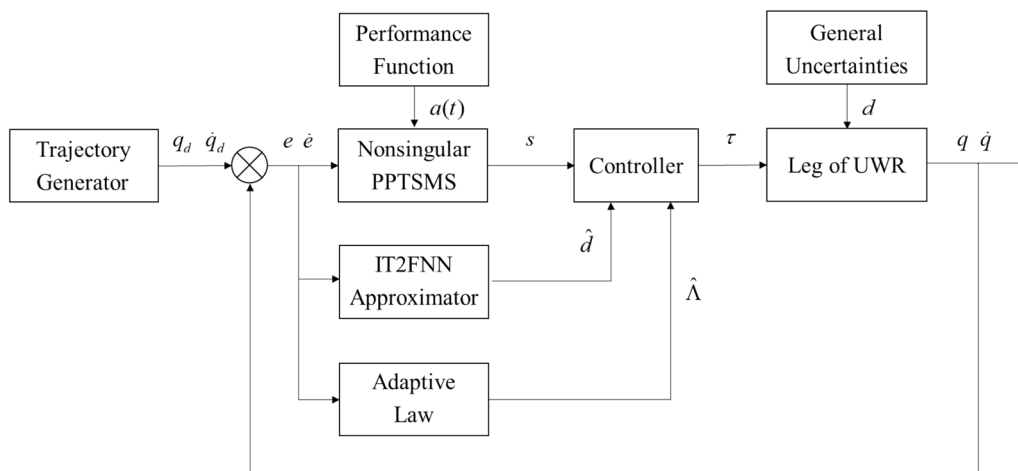When state variables arrive at the sliding surface $s_i = 0$, from (10), we have

Fig. 5 Nonsingular PPTSMC strategy

$$\frac{\mathrm{d}e_i}{\mathrm{d}t} = \frac{k_1 \sigma(e_i)}{k_2 \ln|e_i/a_i(t)|} \tag{15}$$

and the solution of (15) T_{si} satisfies

$$T_{si} = \int_{e_i(0)}^{0} \frac{k_2 \ln|e_i/a_i(t)|}{k_1 \sigma(e_i)} de_i < \int_{a_i(0)}^{0} \frac{k_2 \ln|e_i/a_i(0)|}{k_1 \sigma(e_i)} de_i$$

$$= \frac{k_2}{k_1 \sigma(\xi_i)} \int_{a_i(0)}^{0} \ln|e_i/a_i(0)| de_i = \frac{k_2 a_i(0)}{k_1 \sigma(\xi_i)} \tag{16}$$

From (16), T_{si} is independent of the initial conditions. Above all, the proof of Lemma 3 is completed.

Remark 5 $\sigma(x)$ can be considered as a smooth sign function. What's more, the higher the value of α is, the fewer the differences between $\sigma(x)$ and $\mathrm{sgn}(x)$ there are. When the value of α is high enough, we can practically regard $\sigma(x)$ as $\mathrm{sgn}(x)$, and then we have $\sigma(\xi_i) = 1$ and $T_{si} = k_2 a_i(0)/k_1$.

We propose a nonsingular PPTSMC strategy based on (10) as follows

$$\tau = \tau_n + \tau_d \tag{17}$$

$$\tau_n = \mathbf{C}(\mathbf{q}, \dot{\mathbf{q}})\dot{\mathbf{q}} + \mathbf{g}(\mathbf{q})$$
$$+ \mathbf{M}(\mathbf{q})\left(\ddot{\mathbf{q}}_d - \frac{1}{k_2}(\boldsymbol{\psi} + \kappa \mathrm{sig}^{\mu}(\mathbf{s}) + \lambda \mathrm{sig}^{\nu}(\mathbf{s}))\right) \tag{18}$$

$$\tau_d = -\mathbf{M}(\mathbf{q})\left(\hat{\mathbf{W}}^{\mathrm{T}} \varphi + \hat{\Lambda} \mathrm{sgn}(\mathbf{s})\right) \tag{19}$$

where $\kappa, \lambda > 0, 0 < \mu < 1, \nu > 1$, $\boldsymbol{\psi} = [\psi_1, \psi_2, \ldots, \psi_p]^{\mathrm{T}}$, $\mathbf{s} = [s_1, s_2, \ldots, s_p]^{\mathrm{T}}$, $\hat{\mathbf{W}}$ and $\hat{\Lambda}$ denote the estimation values of $\mathbf{W}$ and Λ, respectively, and adaptive laws are design as follows

$$\dot{\hat{\mathbf{W}}} = \gamma_1\left(\varphi \mathbf{s}^{\mathrm{T}} - \delta_1 \hat{\mathbf{W}}\right) \tag{20}$$

$$\dot{\hat{\Lambda}} = \gamma_2\left(\|\mathbf{s}\| - \delta_2 \hat{\Lambda}\right) \tag{21}$$

where $\gamma_1, \gamma_2, \delta_1, \delta_2 > 0$.

The nonsingular PPTSMC strategy is shown in Fig. 5.

Theorem 1 *For the UWR's leg* (3) *with external disturbances, error constraints, and actuator faults, if Assumptions* 1, 23, 45 *hold, the nonsingular PPTSMC strategy designed as* (17, 18, 19, 20, 21) *guarantees that the tracking error* **e** *will converge to a neighborhood of the origin in fixed-time. Meanwhile, the constraints on position tracking errors* $a_i(t)$, $i = 1, 2, \ldots, p$ *are never violated.*

Proof
Step 1: Consider the following Lyapunov function

$$V_1 = \frac{1}{2}\mathbf{s}^{\mathrm{T}}\mathbf{s} + \frac{k_2}{2\gamma_1}\mathrm{tr}\left(\tilde{\mathbf{W}}^{\mathrm{T}}\tilde{\mathbf{W}}\right) + \frac{k_2}{2\gamma_2}\tilde{\Lambda}^2 \tag{22}$$

where $\tilde{\mathbf{W}} = \mathbf{W} - \hat{\mathbf{W}}$, $\tilde{\Lambda} = \Lambda - \hat{\Lambda}$.

Taking the derivative of (22), we have

$$\dot{V}_1 = -\kappa \mathbf{s}^{\mathrm{T}}\mathrm{sig}^{\mu}(\mathbf{s}) - \lambda \mathbf{s}^{\mathrm{T}}\mathrm{sig}^{\nu}(\mathbf{s}) + k_2\left(\mathbf{s}^{\mathrm{T}}\tilde{\mathbf{W}}^{\mathrm{T}}\varphi - \mathrm{tr}\left(\tilde{\mathbf{W}}^{\mathrm{T}}\varphi \mathbf{s}^{\mathrm{T}}\right)\right)$$
$$+ k_2\delta_1\mathrm{tr}\left(\tilde{\mathbf{W}}^{\mathrm{T}}\hat{\mathbf{W}}\right) + k_2\delta_2\tilde{\Lambda}\hat{\Lambda} + k_2\left(\mathbf{s}^{\mathrm{T}}\boldsymbol{\theta} - \Lambda\|\mathbf{s}\|\right)$$
$$\leq -\kappa \mathbf{s}^{\mathrm{T}}\mathrm{sig}^{\mu}(\mathbf{s}) - \lambda \mathbf{s}^{\mathrm{T}}\mathrm{sig}^{\nu}(\mathbf{s}) + k_2\left(\mathbf{s}^{\mathrm{T}}\tilde{\mathbf{W}}^{\mathrm{T}}\varphi - \mathrm{tr}\left(\tilde{\mathbf{W}}^{\mathrm{T}}\varphi \mathbf{s}^{\mathrm{T}}\right)\right)$$
$$+ k_2\delta_1\mathrm{tr}\left(\tilde{\mathbf{W}}^{\mathrm{T}}\hat{\mathbf{W}}\right) + k_2\delta_2\tilde{\Lambda}\hat{\Lambda} \tag{23}$$

where $\mathbf{s}^{\mathrm{T}}\tilde{\mathbf{W}}^{\mathrm{T}}\varphi$ is a scalar, then we can obtain

$$\mathbf{s}^{\mathrm{T}}\tilde{\mathbf{W}}^{\mathrm{T}}\varphi = \mathrm{tr}\left(\mathbf{s}^{\mathrm{T}}\tilde{\mathbf{W}}^{\mathrm{T}}\varphi\right) = \mathrm{tr}\left(\tilde{\mathbf{W}}^{\mathrm{T}}\varphi \mathbf{s}^{\mathrm{T}}\right) \tag{24}$$

Notice that these inequalities hold

$$\mathrm{tr}\left(\tilde{\mathbf{W}}^{\mathrm{T}}\hat{\mathbf{W}}\right) = \mathrm{tr}\left(\tilde{\mathbf{W}}^{\mathrm{T}}\mathbf{W}\right) - \mathrm{tr}\left(\tilde{\mathbf{W}}^{\mathrm{T}}\tilde{\mathbf{W}}\right) \leq \frac{1}{2}\mathrm{tr}\left(\mathbf{W}^{\mathrm{T}}\mathbf{W}\right)$$
$$- \frac{1}{2}\mathrm{tr}\left(\tilde{\mathbf{W}}^{\mathrm{T}}\tilde{\mathbf{W}}\right) \tag{25}$$

$$\tilde{\varLambda}\hat{\varLambda} = \tilde{\varLambda}\varLambda - \tilde{\varLambda}^2 \leq \frac{1}{2}\varLambda^2 - \frac{1}{2}\tilde{\varLambda}^2 \tag{26}$$

For $x \geq 0$, the following inequality holds

$$-x^{\frac{v+1}{2}} \leq -x + \left(\frac{2}{v+1}\right)^{\frac{2}{v-1}} - \left(\frac{2}{v+1}\right)^{\frac{v+1}{v-1}} \tag{27}$$

Substituting (24, 25, 26) into (23) and combining with (27), we have

$$
\begin{aligned}
\dot{V}_1 \leq &-\kappa\mathbf{s}^{\mathrm{T}}\mathrm{sig}^{\mu}(\mathbf{s}) - \lambda\mathbf{s}^{\mathrm{T}}\mathrm{sig}^{v}(\mathbf{s}) - \frac{k_2\delta_1}{2}\mathrm{tr}\left(\tilde{\mathbf{W}}^{\mathrm{T}}\tilde{\mathbf{W}}\right) - \frac{k_2\delta_2}{2}\tilde{\varLambda}^2 \\
&+ \frac{k_2\delta_1}{2}\mathrm{tr}\left(\mathbf{W}^{\mathrm{T}}\mathbf{W}\right) + \frac{k_2\delta_2}{2}\varLambda^2 \\
\leq &-\lambda\mathbf{s}^{\mathrm{T}}\mathrm{sig}^{v}(\mathbf{s}) - \frac{k_2\delta_1}{2}\mathrm{tr}\left(\tilde{\mathbf{W}}^{\mathrm{T}}\tilde{\mathbf{W}}\right) - \frac{k_2\delta_2}{2}\tilde{\varLambda}^2 \\
&+ \frac{k_2\delta_1}{2}\mathrm{tr}\left(\mathbf{W}^{\mathrm{T}}\mathbf{W}\right) + \frac{k_2\delta_2}{2}\varLambda^2 \\
\leq &-\lambda\mathbf{s}^{\mathrm{T}}\mathbf{s} - \frac{k_2\delta_1}{2}\mathrm{tr}\left(\tilde{\mathbf{W}}^{\mathrm{T}}\tilde{\mathbf{W}}\right) - \frac{k_2\delta_2}{2}\tilde{\varLambda}^2 + \vartheta_1 \\
\leq &-\sigma_1 V_1 + \vartheta_1
\end{aligned} \tag{28}
$$

where $\sigma_1 = \min\{2\lambda, \delta_1\gamma_1, \delta_2\gamma_2\}$, and $\vartheta_1 = p\lambda\left(\left(\frac{2}{v+1}\right)^{\frac{2}{v-1}} - \left(\frac{2}{v+1}\right)^{\frac{v+1}{v-1}}\right) + \frac{k_2\delta_1}{2}\mathrm{tr}\left(\mathbf{W}^{\mathrm{T}}\mathbf{W}\right) + \frac{k_2\delta_2}{2}\varLambda^2$.
Thus $\mathbf{s}, \tilde{\mathbf{W}}, \tilde{\varLambda}$ are uniformly ultimately bounded, and there are positive constants Δ_1 and Δ_2 such that $\mathrm{tr}\left(\tilde{\mathbf{W}}^{\mathrm{T}}\tilde{\mathbf{W}}\right) \leq \Delta_1$ and $\tilde{\varLambda}^2 \leq \Delta_2$.

Step 2: For $x \geq 0$, the following inequality holds

$$x^{\frac{\mu+1}{2}} - x \leq \left(\frac{\mu+1}{2}\right)^{\frac{\mu+1}{1-\mu}} - \left(\frac{\mu+1}{2}\right)^{\frac{2}{1-\mu}} \tag{29}$$

Combining with (24, 25, 26, 29), and Lemma 2, (23) can be rewritten as

$$
\begin{aligned}
\dot{V}_1 \leq &-\kappa\mathbf{s}^{\mathrm{T}}\mathrm{sig}^{\mu}(\mathbf{s}) - \lambda\mathbf{s}^{\mathrm{T}}\mathrm{sig}^{v}(\mathbf{s}) - \frac{k_2\delta_1}{2}\mathrm{tr}\left(\tilde{\mathbf{W}}^{\mathrm{T}}\tilde{\mathbf{W}}\right) - \frac{k_2\delta_2}{2}\tilde{\varLambda}^2 + \frac{k_2\delta_1}{2}\mathrm{tr}\left(\mathbf{W}^{\mathrm{T}}\mathbf{W}\right) + \frac{k_2\delta_2}{2}\varLambda^2 \\
\leq &-2^{\frac{\mu+1}{2}}\kappa\left(\frac{1}{2}\mathbf{s}^{\mathrm{T}}\mathbf{s}\right)^{\frac{\mu+1}{2}} - (\delta_1\gamma_1)^{\frac{\mu+1}{2}}\left(\frac{k_2}{2\gamma_1}\mathrm{tr}\left(\tilde{\mathbf{W}}^{\mathrm{T}}\tilde{\mathbf{W}}\right)\right)^{\frac{\mu+1}{2}} - (\delta_2\gamma_2)^{\frac{\mu+1}{2}}\left(\frac{k_2}{2\gamma_2}\tilde{\varLambda}^2\right)^{\frac{\mu+1}{2}} \\
&-2^{\frac{v+1}{2}}\lambda p^{\frac{1-v}{2}}\left(\frac{1}{2}\mathbf{s}^{\mathrm{T}}\mathbf{s}\right)^{\frac{v+1}{2}} - \left(\frac{k_2}{2\gamma_1}\mathrm{tr}\left(\tilde{\mathbf{W}}^{\mathrm{T}}\tilde{\mathbf{W}}\right)\right)^{\frac{v+1}{2}} - \left(\frac{k_2}{2\gamma_2}\tilde{\varLambda}^2\right)^{\frac{v+1}{2}} + \vartheta_2 \\
\leq &-\sigma_2 V_1^{\frac{\mu+1}{2}} - \sigma_3 V_1^{\frac{v+1}{2}} + \vartheta_2
\end{aligned} \tag{30}
$$

where $\sigma_2 = \min\left\{2^{\frac{\mu+1}{2}}\kappa, (\delta_1\gamma_1)^{\frac{\mu+1}{2}}, (\delta_2\gamma_2)^{\frac{\mu+1}{2}}\right\}$, $\sigma_3 = 3^{\frac{1-v}{2}}\min\left\{2^{\frac{v+1}{2}}\lambda p^{\frac{1-v}{2}}, 1\right\}$, and $\vartheta_2 = \frac{k_2\delta_1}{2}\mathrm{tr}\left(\mathbf{W}^{\mathrm{T}}\mathbf{W}\right) + \frac{k_2\delta_2}{2}\varLambda^2 + 2\left(\frac{\mu+1}{2}\right)^{\frac{\mu+1}{1-\mu}} - 2\left(\frac{\mu+1}{2}\right)^{\frac{2}{1-\mu}} + \left(\frac{k_2\Delta_1}{2\gamma_1}\right)^{\frac{v+1}{2}} + \left(\frac{k_2\Delta_2}{2\gamma_2}\right)^{\frac{v+1}{2}}$.

According to Lemma 1, the state variables $\mathbf{q}$ and $\dot{\mathbf{q}}$ of the UWR's leg will converge to the sliding surface $\mathbf{s} = 0_p$ in the fixed time T_{v1}, and T_{v1} satisfies

$$T_{v1} \leq \frac{2}{\sigma_2\theta_1(1-\mu)} + \frac{2}{\sigma_3\theta_1(v-1)} \tag{31}$$

where $0 < \theta_1 < 1$. From (31) and Lemma 3, the global settling time T_1 satisfies

$$
\begin{aligned}
T_1 < &\frac{2}{\sigma_2\theta_1(1-\mu)} + \frac{2}{\sigma_3\theta_1(v-1)} + \max\left(\frac{k_2a_i(0)}{k_1\sigma(\alpha\xi_i)}\right), i \\
&= 1, 2, \ldots, p
\end{aligned} \tag{32}
$$

Therefore, the tracking errors $\mathbf{e}$ of the UWR's leg will converge to a neighborhood of the origin in the fixed time, and the proof of Theorem 1 is completed.

3.3 Design of Integral PPTSMC Strategy

To reduce steady-state errors, we rewrite (10) as follow

$$s_{Ii} = \int\left(-\frac{k_1\sigma(\alpha e_i)}{\ln|e_i/a_i(t)|} + k_2\dot{e}_i\right) \tag{33}$$

Comparing (33) with (10), we can obtain the following lemma according to Lemma 3.

Lemma 4 *Tracking errors $\mathbf{e}$ never violate the constraints of performance functions due to the PPTSMS (33). Once state variables reach the surface $s_{Ii} = 0$, tracking errors are guaranteed to converge in a fixed time T_{sIi}. The settling time T_{sIi} is independent of the initial conditions, and satisfies*

$$T_{sIi} < \frac{k_2a_i(0)}{k_1\sigma(\xi_i)} \tag{34}$$

We propose an integral PPTSMC strategy based on (33) as follows

$$\boldsymbol{\tau} = \boldsymbol{\tau}_n + \boldsymbol{\tau}_d \tag{35}$$

$$
\begin{aligned}
\boldsymbol{\tau}_n = &\mathbf{C}(\mathbf{q}, \dot{\mathbf{q}})\dot{\mathbf{q}} + \mathbf{g}(\mathbf{q}) \\
&+ \mathbf{M}(\mathbf{q})\left(\ddot{\mathbf{q}}_d + \frac{1}{k_2}\left(\dot{\boldsymbol{\zeta}} - \mathbf{s}_I - \boldsymbol{\psi} - \kappa_2\mathrm{sig}^{\mu}(\mathbf{s} - \boldsymbol{\zeta}) - \lambda_2\mathrm{sig}^{v}(\mathbf{s} - \boldsymbol{\zeta})\right)\right)
\end{aligned} \tag{36}
$$

$$\boldsymbol{\tau}_d = -\mathbf{M}(\mathbf{q})\left(\hat{\mathbf{W}}^{\mathrm{T}}\varphi + \hat{\varLambda}\mathrm{sgn}(\mathbf{s} - \boldsymbol{\zeta})\right) \tag{37}$$

where $\mathbf{s}_I = \left[s_{I1}, s_{I2}, \ldots, s_{Ip}\right]^{\mathrm{T}}$, $\boldsymbol{\zeta} = -\kappa_1\mathrm{sig}^{\mu}(\mathbf{s}_I) - \lambda_1\mathrm{sig}^{v}(\mathbf{s}_I)$ is a virtual control variable, and adaptive laws are design as follows

$$\dot{\hat{\mathbf{W}}} = \gamma_1\left(\varphi(\mathbf{s} - \boldsymbol{\zeta})^{\mathrm{T}} - \delta_1\hat{\mathbf{W}}\right) \tag{38}$$

$$\dot{\hat{\varLambda}} = \gamma_2\left(\|\mathbf{s} - \boldsymbol{\zeta}\| - \delta_2\hat{\varLambda}\right) \tag{39}$$
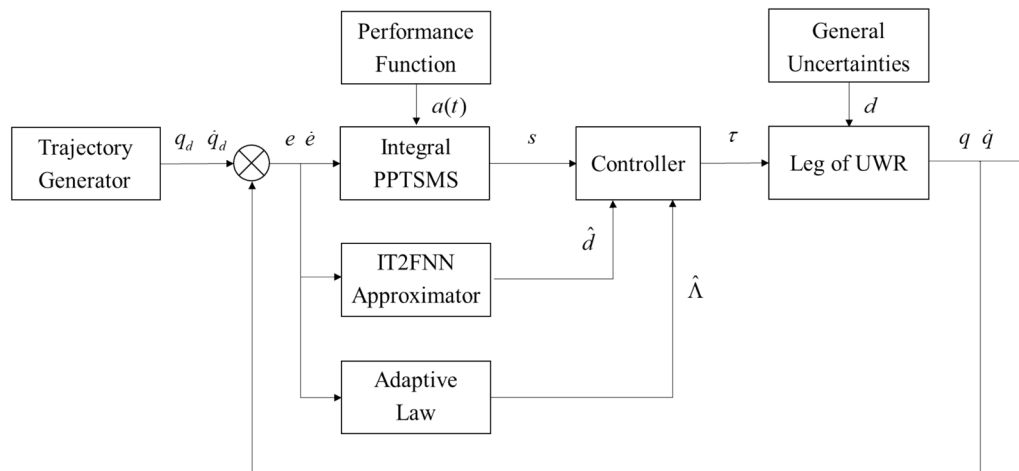
Fig. 6 Integral PPTSMC strategy

where $\gamma_1, \gamma_2, \delta_1, \delta_2 > 0$.

The integral PPTSMC strategy is shown in Fig. 6.

Theorem 2 *For the UWR's leg which is described by* (3), *the external disturbances, error constraints, and actuator faults are considered. If Assumptions* 1, 23, 45 *hold, the integral PPTSMC strategy designed as* (35, 36, 37, 38, 39) *guarantees the global fixed-time stability. Meanwhile, the constraints* $a_i(t), i = 1, 2, \ldots, p$ *on position tracking error* **e** *are never violated.*

Proof

Step 1: Consider the following Lyapunov function

$$V_2 = \frac{1}{2}\mathbf{s}_I^{\mathrm{T}}\mathbf{s}_I + \frac{1}{2}(\mathbf{s} - \boldsymbol{\zeta})^{\mathrm{T}}(\mathbf{s} - \boldsymbol{\zeta}) + \frac{k_2}{2\gamma_1}\mathrm{tr}\left(\tilde{\mathbf{W}}^{\mathrm{T}}\tilde{\mathbf{W}}\right) + \frac{k_2}{2\gamma_2}\tilde{\Lambda}^2 \tag{40}$$

Taking the derivative of (40) from (24, 25, 26, 27), we have

$$
\begin{aligned}
\dot{V}_2 &= -\kappa_1\mathbf{s}_I^{\mathrm{T}}\mathrm{sig}^\mu(\mathbf{s}_I) - \lambda_1\mathbf{s}_I^{\mathrm{T}}\mathrm{sig}^v(\mathbf{s}_I) - \kappa_2(\mathbf{s} - \boldsymbol{\zeta})^{\mathrm{T}}\mathrm{sig}^\mu(\mathbf{s} - \boldsymbol{\zeta}) \\
&\quad - \lambda_2(\mathbf{s} - \boldsymbol{\zeta})^{\mathrm{T}}\mathrm{sig}^v(\mathbf{s} - \boldsymbol{\zeta}) + k_2\delta_1\mathrm{tr}\left(\tilde{\mathbf{W}}^{\mathrm{T}}\hat{\mathbf{W}}\right) + k_2\delta_2\tilde{\Lambda}\hat{\Lambda} \\
&\quad + k_2\left((\mathbf{s} - \boldsymbol{\zeta})^{\mathrm{T}}\boldsymbol{\theta} - \Lambda\|\mathbf{s} - \boldsymbol{\zeta}\|\right) \\
&\leq -\lambda_1\mathbf{s}_I^{\mathrm{T}}\mathrm{sig}^v(\mathbf{s}_I) - \lambda_2(\mathbf{s} - \boldsymbol{\zeta})^{\mathrm{T}}\mathrm{sig}^v(\mathbf{s} - \boldsymbol{\zeta}) \\
&\quad - \frac{k_2\delta_1}{2}\mathrm{tr}\left(\tilde{\mathbf{W}}^{\mathrm{T}}\tilde{\mathbf{W}}\right) - \frac{k_2\delta_2}{2}\tilde{\Lambda}^2 \\
&\quad + \frac{k_2\delta_1}{2}\mathrm{tr}\left(\mathbf{W}^{\mathrm{T}}\mathbf{W}\right) + \frac{k_2\delta_2}{2}\Lambda^2 \\
&\leq -\lambda_1\mathbf{s}_I^{\mathrm{T}}\mathbf{s}_I - \lambda_2(\mathbf{s} - \boldsymbol{\zeta})^{\mathrm{T}}(\mathbf{s} - \boldsymbol{\zeta}) - \frac{k_2\delta_1}{2}\mathrm{tr}\left(\tilde{\mathbf{W}}^{\mathrm{T}}\tilde{\mathbf{W}}\right) \\
&\quad - \frac{k_2\delta_2}{2}\tilde{\Lambda}^2 + \vartheta_3 \\
&\leq -\sigma_4 V_2 + \vartheta_3
\end{aligned}
$$

$$\tag{41}$$

where $\sigma_4 = \min\{2\lambda_1, 2\lambda_2, \delta_1\gamma_1, \delta_2\gamma_2\}$, and $\vartheta_3 = p(\lambda_1 + \lambda_2)\left(\left(\frac{2}{v+1}\right)^{\frac{2}{v-1}} - \left(\frac{2}{v+1}\right)^{\frac{v+1}{v-1}}\right) + \frac{k_2\delta_1}{2}\mathrm{tr}\left(\mathbf{W}^{\mathrm{T}}\mathbf{W}\right) + \frac{k_2\delta_2}{2}\Lambda^2$.

Thus, $\mathbf{s}_I, \mathbf{s}, \tilde{\mathbf{W}}, \tilde{\Lambda}$ are uniformly ultimately bounded, and there are positive constants Δ_3 and Δ_4 such that $\mathrm{tr}\left(\tilde{\mathbf{W}}^{\mathrm{T}}\tilde{\mathbf{W}}\right) \leq \Delta_3$ and $\tilde{\Lambda}^2 \leq \Delta_4$.

Step 2: Combining with (24, 25, 26, 29), and Lemma 2, (41) can be rewritten as

$$
\begin{aligned}
\dot{V}_2 &\leq -2^{\frac{\mu+1}{2}}\kappa_1\left(\frac{1}{2}\mathbf{s}_I^{\mathrm{T}}\mathbf{s}_I\right)^{\frac{\mu+1}{2}} - 2^{\frac{\mu+1}{2}}\kappa_2\left(\frac{1}{2}(\mathbf{s} - \boldsymbol{\zeta})^{\mathrm{T}}(\mathbf{s} - \boldsymbol{\zeta})\right)^{\frac{\mu+1}{2}} \\
&\quad - (\delta_1\gamma_1)^{\frac{\mu+1}{2}}\left(\frac{k_2}{2\gamma_1}\mathrm{tr}\left(\tilde{\mathbf{W}}^{\mathrm{T}}\tilde{\mathbf{W}}\right)\right)^{\frac{\mu+1}{2}} - (\delta_2\gamma_2)^{\frac{\mu+1}{2}}\left(\frac{k_2}{2\gamma_2}\tilde{\Lambda}^2\right)^{\frac{\mu+1}{2}} \\
&\quad - 2^{\frac{v+1}{2}}\lambda_1 p^{\frac{1-v}{2}}\left(\frac{1}{2}\mathbf{s}_I^{\mathrm{T}}\mathbf{s}_I\right)^{\frac{v+1}{2}} - 2^{\frac{v+1}{2}}\lambda_2 p^{\frac{1-v}{2}}\left(\frac{1}{2}(\mathbf{s} - \boldsymbol{\zeta})^{\mathrm{T}}(\mathbf{s} - \boldsymbol{\zeta})\right)^{\frac{v+1}{2}} \\
&\quad - \left(\frac{k_2}{2\gamma_1}\mathrm{tr}\left(\tilde{\mathbf{W}}^{\mathrm{T}}\tilde{\mathbf{W}}\right)\right)^{\frac{v+1}{2}} - \left(\frac{k_2}{2\gamma_2}\tilde{\Lambda}^2\right)^{\frac{v+1}{2}} + \vartheta_4 \\
&\leq -\sigma_5 V_2^{\frac{\mu+1}{2}} - \sigma_6 V_2^{\frac{v+1}{2}} + \vartheta_4
\end{aligned}
$$

$$\tag{42}$$

Where $\sigma_5 = \min\left\{2^{\frac{\mu+1}{2}}\kappa_1, 2^{\frac{\mu+1}{2}}\kappa_2, (\delta_1\gamma_1)^{\frac{\mu+1}{2}}, (\delta_2\gamma_2)^{\frac{\mu+1}{2}}\right\}$, $\sigma_6 = 4^{\frac{1-v}{2}}\min\left\{2^{\frac{v+1}{2}}\lambda_1 p^{\frac{1-v}{2}}, 2^{\frac{v+1}{2}}\lambda_2 p^{\frac{1-v}{2}}, 1\right\}$, $\vartheta_4 = \frac{k_2\delta_1}{2}\mathrm{tr}\left(\mathbf{W}^{\mathrm{T}}\mathbf{W}\right) + \frac{k_2\delta_2}{2}\Lambda^2 + 2\left(\frac{\mu+1}{2}\right)^{\frac{\mu+1}{1-\mu}} - 2\left(\frac{\mu+1}{2}\right)^{\frac{2}{1-\mu}} + \left(\frac{k_2\Delta_3}{2\gamma_1}\right)^{\frac{v+1}{2}} + \left(\frac{k_2\Delta_4}{2\gamma_2}\right)^{\frac{v+1}{2}}$.

According to Lemma 1, the state variables **q** and $\dot{\mathbf{q}}$ of the UWR's leg will converge to sliding surface $\mathbf{s}_I = 0_p$ in the fixed time T_{v2}, and T_{v2} satisfies

$$T_{v2} \leq \frac{2}{\sigma_5\theta_2(1-\mu)} + \frac{2}{\sigma_6\theta_2(v-1)} \tag{43}$$

where $0 < \theta_2 < 1$. From (43) and Lemma 4, the global settling time T_1 satisfies

$$T_2 < \frac{2}{\sigma_5\theta_2(1-\mu)} + \frac{2}{\sigma_6\theta_2(v-1)} + \max\left(\frac{k_2 a_i(0)}{k_1\sigma(\alpha\xi_i)}\right), \ i$$
$$= 1, 2, \ldots, p \tag{44}$$

Thus the tracking error $\mathbf{e}$ of UWR's leg will converge to zero in a fixed time, which implies the proof of Theorem 2 is completed.

4 Numerical Simulations

To illustrate the effectiveness of the two proposed control strategies, simulation results for a two links UWR's leg are presented in this section. The dynamics of the two links UWR's leg can be described by (3), and the details are as follows

$$\mathbf{q} = [q_1, q_2]^T,$$
$$\mathbf{M}(\mathbf{q}) = \begin{bmatrix} \theta_1 + \theta_2 + 2\theta_3\cos q_2 & \theta_2 + \theta_3\cos q_2 \\ \theta_2 + \theta_3\cos q_2 & \theta_2 \end{bmatrix},$$
$$\mathbf{C}(\mathbf{q}, \dot{\mathbf{q}}) = \begin{bmatrix} -\theta_3(\sin q_2)\dot{q}_2 & -\theta_3(\sin q_2)(\dot{q}_1 + \dot{q}_2) \\ \theta_3(\sin q_2)\dot{q}_1 & 0 \end{bmatrix},$$
$$\mathbf{G}(\mathbf{q}) = \begin{bmatrix} \theta_4 g\cos q_1 + \theta_5 g\cos(q_1 + q_2) \\ \theta_5 g\cos(q_1 + q_2) \end{bmatrix},$$
$$\boldsymbol{\rho}(t) = \mathrm{diag}(\rho_1(t), \rho_2(t)), \quad \boldsymbol{\tau}_b(t) = [\tau_{b1}(t), \tau_{b2}(t)]^T,$$
$$\boldsymbol{\omega} = 5\% \cdot [\mathbf{M}(\mathbf{q})\ddot{\mathbf{q}} + \mathbf{C}(\mathbf{q}, \dot{\mathbf{q}})\dot{\mathbf{q}} + \mathbf{g}(\mathbf{q})]$$

where $\theta_1 = J_1 + m_2 l_1^2$, $\theta_2 = 0.25 m_2 l_2^2 + J_2$, $\theta_3 = 0.5 m_2 l_1 l_2$, $\theta_4 = (0.5 m_1 + m_2) l_1$, $\theta_5 = 0.5 m_2 l_2$, $g = 9.8 \text{ m s}^{-2}$ is the gravitational acceleration, $J_1 = 0.21 \text{ kg m}^2$, $J_2 = 0.42 \text{ kg} \cdot \text{m}^2$, $m_1 = 1.02 \text{ kg}$, $m_2 = 1.12 \text{ kg}$, $l_1 = l_2 = 1 \text{ m}$ denote the moments of inertia, masses, and lengths of each link, respectively.

4.1 Simulation Results For Nonsingular PPTSMC Strategy

We consider the following case. For each link of UWR's leg, the initial values of state variables are given as $q_1(0) = \frac{4}{5}\pi \text{ rad}$, $q_2(0) = -\frac{2}{3}\pi \text{ rad}$, $\dot{q}_1(0) = \dot{q}_2(0) = 0 \text{ rad s}^{-1}$, and the desired trajectories are set as $q_1(t) = \frac{\pi}{20}\sin(\pi t) + \frac{\pi}{10} \text{ rad}$, $q_2(t) = \frac{\pi}{15}\sin(\pi t) \text{ rad}$. We assume that actuators will have fault once $t=10$ s, and the details of faults are as follows

$$\rho_1(t) = \rho_2(t) = \begin{cases} 1 & t < 10 \text{ s} \\ 0.6 & t \geq 10 \text{ s} \end{cases}, \ \tau_{b1}(t)$$
$$= \begin{cases} 0 & t < 10 \text{ s} \\ 15\text{N} & t \geq 10 \text{ s} \end{cases}, \ \tau_{b2}(t) = \begin{cases} 0 & t < 10 \text{ s} \\ 5\text{N} & t \geq 10 \text{ s} \end{cases}$$

For IT2FNN approximator, we choose Gaussian membership functions and the following rules

$$\hat{X}_k^i = \begin{cases} \mu_{\underline{X}_k^i}(x_k) = \exp\left(-\frac{(x_k - c_k^i)^2}{2\sigma_{1k}^i}\right) \\ \mu_{\overline{X}_k^i}(x_k) = \exp\left(-\frac{(x_k - c_k^i)^2}{2\sigma_{2k}^i}\right) \end{cases} \tag{45}$$

where $i = 1, 2, 3, 4$, $k = 1, 2, 3, 4$, $\sigma_{1k}^i = 1$, $\sigma_{2k}^i = 2$, $c_1^1 = c_2^1 = c_3^1 = c_4^1 = c_1^2 = c_2^2 = c_3^3 = c_4^3 = 4$, and $c_3^2 = c_4^2 = c_1^3 = c_2^3 = c_1^4 = c_2^4 = c_3^4 = c_4^4 = -4$. The initial value of $\hat{\mathbf{W}}$ is $0_{4\times2}$, and the initial value of $\hat{\Lambda}$ is 0. The following performance function is chosen

$$a_1(t) = a_2(t) = b_1\exp(-b_2 t) + b_3 \tag{46}$$

where $b_1 = 3$, $b_2 = 1$, and $b_3 = 0.01$.

The parameters of the controller proposed in Sect. 3.2 are selected as $\alpha = 100$, $k_1 = 1$, $k_2 = 1$, $\mu = 0.6$, $v = 1.4$, $\kappa = 30$, $\lambda = 5$, $\gamma_1 = 0.5$, $\gamma_2 = 0.5$, $\delta_1 = 0.5$, and $\delta_2 = 0.5$. The simulation results are shown in Figs. 7, 8, 9, where Figs. 7, 8 denote the tracking errors for the links 1 and link 2 of UWR's leg, respectively, and Fig. 9 denotes the inputs of two joints of UWR's leg.

From Figs. 7, 8, we can find that e_1 and e_2 can converge to a small neighborhood of zero in about two seconds in the control of nonsingular PPTSMC strategy. For the two links of UWR's leg, the initial values of their generalized coordinates are different, so are their desired trajectories.
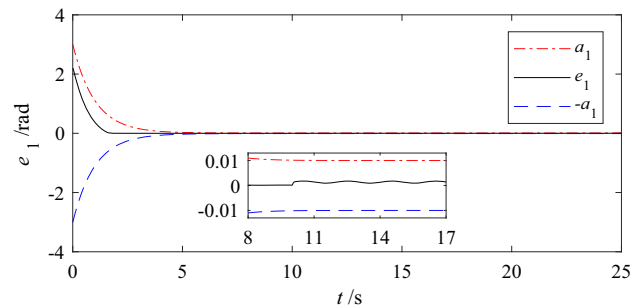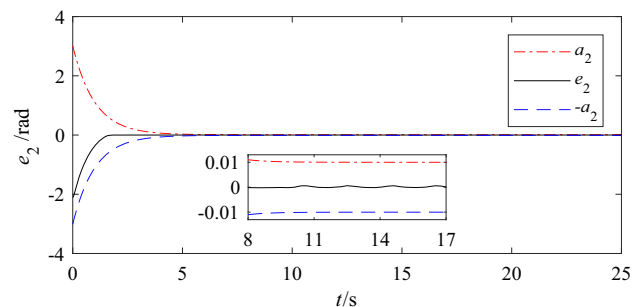

Fig. 7 Tracking error e_1

Fig. 8 Tracking error e_2

Fig. 9 Control input τ

Fig. 10 Tracking error e_1

Fig. 11 Tracking error e_2

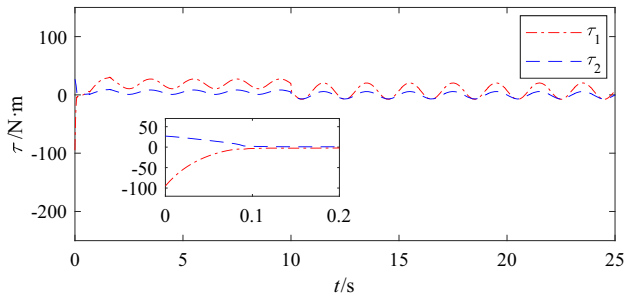**Fig. 12** Control input τ

But the tracking errors can converge to zero within the same time due to the fixed-time stability. Meanwhile, overshoot is small, which indicates the error constraints are guaranteed in the initial stage of control. When the actuators have faults at $t=10$ s, e_1 and e_2 increase but remain bounded. It indicates that those constraints can prescribe the tracking control performances of UWR's leg when the general disturbances vary. Moreover, e_1 and e_2 never violate the constraints of performance functions during the control process, which indicates those constraints are representatives for the tracking performance of UWR's leg. As shown in Fig. 9, the maximum amplitude of control input τ is reached during the initial phase, and τ remains bounded whether actuator faults happened or not. It indicates the feasibility of the nonsingular PPTSMC strategy.

4.2 Simulation results for integral PPTSMC strategy

We consider the same case as Sect. 4.1. The parameters of the controller proposed in Sect. 3.3 are selected as $\alpha = 100$, $k_1 = 1$, $k_2 = 1$, $\mu = 0.6$, $v = 1.4$, $\kappa_1 = 8$, $\kappa_2 = 40$, $\lambda_1 = 10$, $\lambda_2 = 10$, $\gamma_1 = 0.5$, $\gamma_2 = 0.5$, $\delta_1 = 0.5$, and $\delta_2 = 0.5$. The simulation results are shown in Figs. 10, 11, 12, where Figs. 10, 11 denote the tracking errors for the link 1 and link 2 of UWR's leg, respectively, and Fig. 12 denotes the inputs of two joints of UWR's leg.

As we can see from Figs. 10, 11, e_1 and e_2 converge to a small neighborhood of zero in 2 s, which indicates the fixed-time stability is guaranteed. When actuators have faults, the variations of tracking errors are very small and the tracking errors satisfy the error constraints. It indicates that the tracking control accuracy of UWR's leg will not be affected by abrupt disturbances. What's more, high steady-state precision is guaranteed in the control of integral PPTSMC strategy. From Fig. 12, the control input τ remains bounded during the whole control process, although it has an abrupt change at $t=10$ s. It indicates the feasibility of the integral PPTSMC strategy.
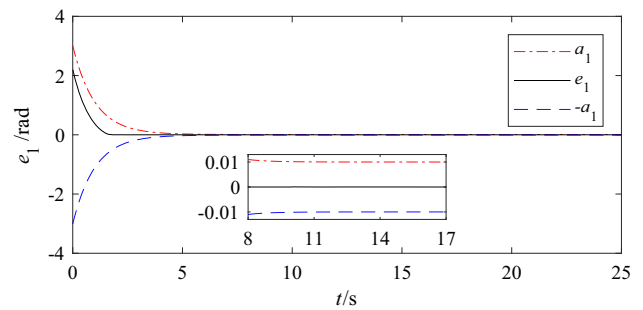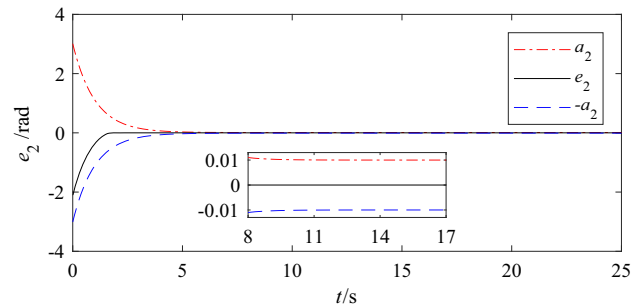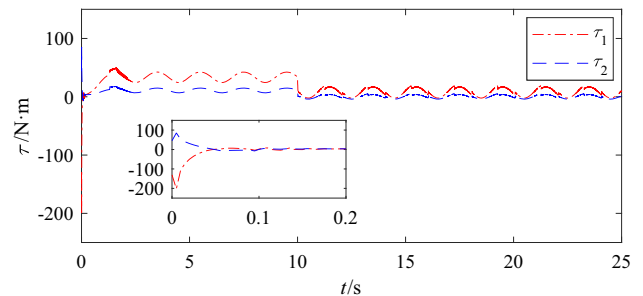
4.3 Performance Comparisons Results

To illustrate the advantages of the two proposed PPTSMC strategies, we compare them with adaptive sliding-mode control (ASMC) strategy (47, 48) and adaptive fast terminal sliding-mode control (AFTSMC) strategy (49, 50). The adaptive laws of ASMC and AFTSMC are selected as the same form of PPTSMC. While the ASMC is asymptotic stability and the AFTSMC is finite-time stability.

$$\tau = \mathbf{C}(\mathbf{q}, \dot{\mathbf{q}})\dot{\mathbf{q}} + \mathbf{g}(\mathbf{q})$$
$$+ \mathbf{M}(\mathbf{q})\left(\ddot{\mathbf{q}}_d - \frac{k_3}{k_4}\dot{\mathbf{e}} - \hat{D}\mathrm{sign}(\mathbf{s}_L) - \lambda_L\mathbf{s}_L\right) \qquad (47)$$

$$\dot{\hat{D}} = \gamma_3 \mathbf{s}_L^{\mathrm{T}} \mathrm{sign}(\mathbf{s}_L) - \gamma_4 \hat{D} \tag{48}$$

where $\mathbf{s}_L = k_3 \mathbf{e} + k_4 \dot{\mathbf{e}}$, D is the unknown bound of nonlinear uncertainties $\mathbf{d}$, $\hat{D}$ denotes the estimation values of D, .

$$\boldsymbol{\tau} = \mathbf{C}(\mathbf{q}, \dot{\mathbf{q}})\dot{\mathbf{q}} + \mathbf{g}(\mathbf{q}) + \mathbf{M}(\mathbf{q})\left(\ddot{\mathbf{q}}_d - \frac{\mu_T}{k_5}\left(\mathrm{sig}^{2-\mu_T}(\dot{\mathbf{e}}) + k_6 v_T |\mathbf{e}|^{v_T} \mathrm{sig}^{2-\mu_T}(\dot{\mathbf{e}})\right)\right) \\ - \mathbf{M}(\mathbf{q})\left(\hat{D}\mathrm{sign}(\mathbf{s}_T) + \lambda_T \mathrm{sig}^{\kappa_T}(\mathbf{s}_T)\right) \tag{49}$$

$$\dot{\hat{D}} = \gamma_5 \mathbf{s}_T^{\mathrm{T}} \mathrm{sign}(\mathbf{s}_T) - \gamma_6 \hat{D} \tag{50}$$

where $\mathbf{s}_T = \mathbf{e} + k_5 \mathrm{sig}^{\mu_T}(\dot{\mathbf{e}}) + k_2 \mathrm{sig}^{v_T}(\mathbf{e})$, $k_5, k_6, \gamma_5, \gamma_6, \lambda_T, > 0$, $1 < \mu_T < v_T < 2$, $0 < \kappa_T < 1$.

For the quantitative analyses of those four control algorithms, we define some indexes as follows

1. *Reference error E: the 1-norm of the tracking error, $E = \|\mathbf{e}\|$.*

2. *Root mean square error E_1: $E_1 = \sqrt{\frac{1}{N}\sum_{i=1}^{N} E^2(t_i)}$, N denotes the step number of simulation, $E(t_i)$ is the reference error in ith step.*

3. *Rough error E_2: the maximum value of reference error E when UWR's leg realizes the tracking control.*

4. *Arrival time T_0: the time when the reference error E converges to the rough error E_2.*

We consider the following simulation setup which is different from Sects. 4.1 and 4.2. For each link of UWR's leg, the initial values of state variables are set as $q_1(0) = \frac{\pi}{15}$ rad, $q_2(0) = \frac{\pi}{10}$ rad, $\dot{q}_1(0) = \dot{q}_2(0) = 0$ rad·s^{-1}, and the desired trajectories are given as $q_1(t) = \frac{\pi}{10}\sin\left(\frac{\pi}{2}t\right) + \frac{\pi}{20}$ rad, $q_2(t) = \frac{\pi}{15}\sin\left(\pi t + \frac{\pi}{5}\right) + \frac{\pi}{10}$ rad. The actuators will have fault on $t = 12$ s, and the fault parameters are

$$\rho_1(t) = \rho_2(t) = \begin{cases} 1 & t < 10 \text{ s} \\ 0.7 & t \geq 10 \text{ s} \end{cases}, \ \tau_{b1}(t) \\ = \begin{cases} 0 & t < 10 \text{ s} \\ 5 \text{ N} & t \geq 10 \text{ s} \end{cases}, \ \tau_{b2}(t) = 0$$

The parameters of nonsingular PPTSMC strategy and integral PPTSMC strategy are the same as those in Sect. 4.1, respectively. The parameters of ASMC strategy are set as $k_3 = 10$, $k_4 = 15$, $\gamma_3 = 1$, $\gamma_4 = 0.1$, $\lambda_T = 1$. The parameters of AFTSMC strategy are given as $k_5 = 15$, $k_6 = 35$, $\gamma_5 = 1$, $\gamma_6 = 0.1$, $\lambda_T = 35$, $\mu_T = 1.8$, $v_T = 1.9$, $\kappa_T = 0.8$. The simulation results are shown in Table 2.

From Table 2, it can be found that the accuracy of the two proposed PPTSMC strategies is higher than the ASMC strategy and the AFTSMC strategy. Although the AFTSMC strategy has the shortest arrival time, its accuracy is not as high as PPTSMC strategies. Among the four

Table 2 The indexes of four algorithms

Algorithm	E_1	E_2	T_0
ASMC	0.1076	0.1026	1.820
AFTSMC	0.09460	0.05569	0.3950
Nonsingular PPTSMC	0.01394	0.005406	0.6100
Integral PPTSMC	0.01240	0.0001272	1.095

algorithms, the integral PPTSMC strategy has the highest accuracy.

5 Conclusion

In the presence of environmental disturbance and unmodeled dynamics, a nonsingular PPTSMC strategy and an integral PPTSMC strategy are proposed to deal with the tracking control problem of UWR's leg with error constraints and actuator faults. Moreover, IT2FNN is utilized to tackle nonlinear uncertainties. Specifically, by introducing a novel PPTSMS, tracking errors never violate the constraints of performance functions. Due to the error constraint performance of PPTSMS, the design processes of controllers based on PPTSMC are simpler than those based on BLF or PP methods. Fixed-time stability is proofed by Lyapunov theory, which indicates the upper bound of settling time is not influenced by the initial values of system states. Simulation results demonstrate that the two proposed control strategies are effective whether the actuator faults happened or not, and the comparative analysis demonstrates that the two proposed control strategies have higher accuracy than ASMC strategy and AFTSMC strategy. In the future, we will try to apply the two proposed control algorithms in this study to some other underwater systems. Moreover, we will improve the performance of our control algorithms, for example, considering the asymmetric error constraints.

References

1. Shukla, A., Karki, H.: Application of robotics in offshore oil and gas industry—a review Part II. Robot. Auton. Syst. **75**, 508–524 (2016)
2. Howe, J.A., Husum, K., Inall, M.E., et al.: Autonomous underwater vehicle (AUV) observations of recent tidewater glacier retreat, western Svalbard. Mar. Geol. **417**, 106009 (2019)
3. Palomer, A., Ridao, P., Ribas, D.: Inspection of an underwater structure using point-cloud SLAM with an AUV and a laser scanner. J. Field. Robot. **36**(8), 1333–1344 (2019)

4. Picardi, G., Laschi, C., Calisti, M.: Model-based open loop control of a multigait legged underwater robot. Mechatronics **55**, 162–170 (2018)

5. Yoo, S., Shim, H., Jun, B.H., et al.: Design of walking and swimming algorithms for a multi-legged underwater robot crabster CR200. Mar. Technol. Soc. J. **50**(5), 74–87 (2016)

6. Li, Z., Yang, C., Ding, N., et al.: Robust adaptive motion control for underwater remotely operated vehicles with velocity constraints. Int. J. Control Autom. Syst. **10**(2), 421–429 (2012)

7. Ghommam, J., Ferik, S.E., Saad, M.: Robust adaptive path-following control of underactuated marine vessel with off-track error constraint. Int. J. Syst. Sci. **49**(7), 1540–1558 (2018)

8. Gao, Z., Guo, G.: Velocity free leader-follower formation control for autonomous underwater vehicles with line-of-sight range and angle constraints. Inf. Sci. **486**, 359–378 (2019)

9. Qin, H., Li, C., Sun, Y., et al.: Adaptive trajectory tracking algorithm of unmanned surface vessel based on anti-windup compensator with full-state constraints. Ocean Eng. **200**, 106906 (2020)

10. Yang, Y., Hua, C., Guan, X.: Finite time control design for bilateral teleoperation system with position synchronization error constrained. IEEE. T. Cybern. **46**(3), 609–619 (2016)

11. Jin, X.: Adaptive fixed-time control for MIMO nonlinear systems with asymmetric output constraints using universal barrier functions. IEEE. Trans. Autom. Control. **64**(7), 3046–3053 (2018)

12. Wang, Z., Liang, B., Sun, Y., et al.: Adaptive fault-tolerant prescribed-time control for teleoperation systems with position error constraints. IEEE Trans. Ind. Inform. **16**(7), 4889–4899 (2020)

13. Zheng, Z., Ruan, L., Zhu, M.: Output-constrained tracking control of an underactuated autonomous underwater vehicle with uncertainties. Ocean. Eng. **175**, 241–250 (2019)

14. Wang, N., Sun, J.C., Er, M.J.: Tracking-error-based universal adaptive fuzzy control for output tracking of nonlinear systems with completely unknown dynamics. IEEE. Trans. Fuzzy Syst. **26**(2), 869–883 (2017)

15. Gundogdu, F.K., Kahraman, C.: A novel fuzzy TOPSIS method using emerging interval-valued spherical fuzzy sets. Eng. Appl. Artif. Intell. **85**, 307–323 (2019)

16. Wu, Z., Karimi, H.R., Dang, C.: An approximation algorithm for graph partitioning via deterministic annealing neural network. Neural Netw. **117**, 191–200 (2019)

17. Wu, Z., Karimi, H.R., Dang, C.: A deterministic annealing neural network algorithm for the minimum concave cost transportation problem. IEEE. Trans. Neural Netw. Learn. Syst. (2019). https://doi.org/10.1109/tnnls.2019.2955137

18. Zhang, Z., Wu, Y.: Adaptive fuzzy tracking control of autonomous underwater vehicles with output constraints. IEEE. Trans. Fuzzy Syst. (2020). https://doi.org/10.1109/TFUZZ.2020.2967294

19. Lin, T.C.: Observer-based robust adaptive interval type-2 fuzzy tracking control of multivariable nonlinear systems. Eng. Appl. Artif. Intell. **23**(3), 386–399 (2010)

20. Moezi, S.A., Zakeri, E., Eghtesad, M.: Optimal adaptive interval type-2 fuzzy fractional-order backstepping sliding mode control method for some classes of nonlinear systems. ISA. Trans. **93**, 23–39 (2019)

21. Golsefid, S.M., Zarandi, M.H., Turksen, I.B., et al.: Multi-central general type-2 fuzzy clustering approach for pattern recognitions. Inf. Sci. **328**, 172–188 (2016)

22. Castillo, O., Melin, P., Ontiveros, E., et al.: A high-speed interval type 2 fuzzy system approach for dynamic parameter adaptation in metaheuristics. Eng. Appl. Artif. Intell. **85**, 666–680 (2019)

23. Wu, D., Mendel, J.M.: Recommendations on designing practical interval type-2 fuzzy systems. Eng. Appl. Artif. Intell. **85**, 182–193 (2019)

24. Kumbasar, T.: Robust Stability analysis and systematic design of single-input interval type-2 fuzzy logic controllers. IEEE Trans. Fuzzy Syst. **24**(3), 675–694 (2016)

25. Yang, L., Liu, Z., Chen, Y., et al.: Energy efficient walking control for biped robots using interval type-2 fuzzy logic systems and optimized iteration algorithm. ISA Trans. **87**, 143–153 (2019)

26. Dian, S., Hu, Y., Zhao, T., et al.: Adaptive backstepping control for flexible-joint manipulator using interval type-2 fuzzy neural network approximator. Nonlinear. Dyn. **97**(2), 1567–1580 (2019)

27. Dong, H., Gao, L., Shen, P., et al.: An interval type-2 fuzzy logic controller design method for hydraulic actuators of a human-like robot by using improved drone squadron optimization. Int. J. Adv. Robot. Syst. **16**(6), 1729881419891553 (2019)

28. Ruizgarcia, G., Hagras, H., Pomares, H., et al.: Toward a fuzzy logic system based on general forms of interval type-2 fuzzy sets. IEEE. Trans. Fuzzy. Syst. **27**(12), 2381–2395 (2019)

29. Lu, X., Zhao, Y., Liu, M., et al.: Self-learning interval type-2 fuzzy neural network controllers for trajectory control of a Delta parallel robot. Neurocomputing. **283**, 107–119 (2017)

30. Zhao, T., Yu, Q., Dian, S., et al.: Non-singleton general type-2 fuzzy control for a two-wheeled self-balancing robot. Int. J. Fuzzy Syst. **21**(6), 1724–1737 (2019)

31. Taghavifar, H., Rakheja, S.: Path-tracking of autonomous vehicles using a novel adaptive robust exponential-like-sliding-mode fuzzy type-2 neural network controller. Mech. Syst. Signal Proc. **130**, 41–55 (2019)

32. Liao, T., Chan, W.S., Yan, J.J., et al.: Distributed adaptive dynamic surface formation control for uncertain multiple quadrotor systems with interval type-2 fuzzy neural networks. Trans. Inst. Meas. Control. **41**(7), 1861–1879 (2019)

33. Zhao, T., Chen, Y., Dian, S., et al.: General type-2 fuzzy gain scheduling PID controller with application to power-line inspection robots. Int. J. Fuzzy Syst. **22**(1), 181–200 (2020)

34. Bechlioulis, C.P., Rovithakis, G.A.: Robust adaptive control of feedback linearizable MIMO nonlinear systems with prescribed performance. IEEE Trans. Autom. Control **53**(9), 2090–2099 (2008)

35. Bechlioulis, C.P., Rovithakis, G.A.: Prescribed performance adaptive control for multi-input multi-output affine in the control nonlinear systems. IEEE. Trans. Autom. Control **55**(5), 1220–1226 (2010)

36. Bechlioulis, C.P., Karras, G.C., Heshmati-Alamdari, S., et al.: Trajectory tracking with prescribed performance for underactuated underwater vehicles under model uncertainties and external disturbances. IEEE. Trans. Control Syst. Technol. **25**(2), 429–440 (2016)

37. Elhaki, O., Shojaei, K.: Neural network-based target tracking control of underactuated autonomous underwater vehicles with a prescribed performance. Ocean. Eng. **167**, 239–256 (2018)

38. Li, J., Du, J., Sun, Y., et al.: Robust adaptive trajectory tracking control of underactuated autonomous underwater vehicles with prescribed performance. Int. J. Robust. Nonlinear. Control **29**(14), 4629–4643 (2019)

39. Shen, C., Shi, Y., Buckham, B.: Trajectory tracking control of an autonomous underwater vehicle using Lyapunov-based model predictive control. IEEE. Trans. Ind. Electron. **65**(7), 5796–5805 (2017)

40. Mahapatra, S., Subudhi, B.: Design and experimental realization of a backstepping nonlinear H∞ control for an autonomous underwater vehicle using a nonlinear matrix inequality approach. Trans. Inst. Meas. Control. **40**(11), 3390–3403 (2018)

41. Wang, J., Wang, C., Wei, Y., et al.: Command filter based adaptive neural trajectory tracking control of an underactuated underwater vehicle in three-dimensional space. Ocean. Eng. **180**, 175–186 (2019)

42. Wu, Z., Jiang, B., Kao, Y.: Finite-time H_∞ filtering for Itô stochastic Markovian jump systems with distributed time-varying delays based on optimisation algorithm. IET. Contr. Theory. Appl. **13**(5), 702–710 (2019)

43. Xu, R., Tang, G., Han, L., et al.: Robust finite-time attitude tracking control of a CMG-based AUV with unknown disturbances and input saturation. IEEE. Access. **7**, 56409–56422 (2019)

44. Patre, B.M., Londhe, P.S., Waghmare, L.M., et al.: Disturbance estimator based non-singular fast fuzzy terminal sliding mode control of an autonomous underwater vehicle. Ocean. Eng. **159**, 372–387 (2018)

45. Polyakov, A.: Nonlinear feedback design for fixed-time stabilization of linear control systems. IEEE Trans. Autom. Control **57**(8), 2106–2110 (2011)

46. Polyakov, A., Efimov, D., Perruquetti, W.: Finite-time and fixed-time stabilization: implicit Lyapunov function approach. Automatica. **51**, 332–340 (2015)

47. Corradini, M.L., Cristofaro, A.: Nonsingular terminal sliding-mode control of nonlinear planar systems with global fixed-time stability guarantees. Automatica. **95**, 561–565 (2018)

48. Gao, Z., Guo, G.: Fixed-time leader-follower formation control of autonomous underwater vehicles with event-triggered intermittent communications. IEEE Access. **6**, 27902–27911 (2018)

49. Kadiyam, J., Parashar, A., Mohan, S., et al.: Actuator fault-tolerant control study of an underwater robot with four rotatable thrusters. Ocean Eng. **197**, 106929 (2020)

50. Sun, Y., Ran, X., Li, Y., et al.: Thruster fault diagnosis method based on Gaussian particle filter for autonomous underwater vehicles. Int. J. Nav. Archit. Ocean Eng. **8**(3), 243–251 (2016)

51. Zeghlache, S., Djerioui, A., Benyettou, L., et al.: Fault tolerant control for modified quadrotor via adaptive type-2 fuzzy backstepping subject to actuator faults. ISA Trans. **87**, 330–345 (2019)

52. Liu, X., Zhang, M., Yao, F.: Adaptive fault tolerant control and thruster fault reconstruction for autonomous underwater vehicle. Ocean Eng. **155**, 10–23 (2018)

53. Xu R, Tang G, Huang D, et al.: Adaptive fault-tolerant attitude control for a CMG-based underwater vehicle. J. Mar. Sci. Technol. 1–8 (2019)

54. Qin, H., Chen, H., Sun, Y., et al.: Distributed finite-time fault-tolerant containment control for multiple ocean Bottom Flying node systems with error constraints. Ocean. Eng. **189**, 106341 (2019)

55. Jiang, B., Hu, Q., Friswell, M.I.: Fixed-time attitude control for rigid spacecraft with actuator saturation and faults. IEEE. Trans. Control. Syst. Technol. **24**(5), 1892–1898 (2016)

56. Zuo, Z.: Nonsingular fixed-time consensus tracking for second-order multi-agent networks. Automatica. **54**, 305–309 (2015)

He Yang Is working toward the M.S. degree in naval architecture and ocean engineering at the Harbin Engineering University. His research interests include bionic robot system control and multiple AUV systems control.
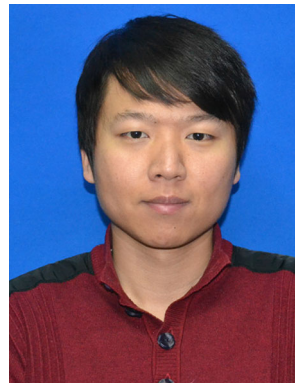
Yanchao Sun Received his B.S. degree in Flight Vehicle Design and Engineering, and M.S. degree and Ph.D. degree in Control Science and Engineering from Harbin Institute of Technology, Harbin, China in 2010, 2012, and 2016, respectively. He is currently an Associate Professor of Science and Technology on Underwater Vehicle Laboratory at the Harbin Engineering University. His research interests include distributed cooperative control of multiple Euler-Lagrange systems, multi-agent system control, and multiple AUV systems control.

Yuang Zhang Is working toward the M.S. degree in naval architecture and ocean engineering at the Harbin Engineering University. His research interests include AUV systems control and nonlinear control.

Hongde Qin Received the Ph.D. degree from Harbin Engineering University, Harbin, China in 2003. He is a Professor and Director of Science and Technology on Underwater Vehicle Laboratory at the Harbin Engineering University. His current research interest involves underwater vehicle system control and bionic robot system control.